Numerical Study of Dynamics of Single Bubbles and Bubble Swarms

Anton Smolianski* Heikki Haario† Pasi Luukka‡

Abstract

A systematic computational study of the dynamics of gas bubbles rising in a viscous liquid is presented. Both the dynamics of single bubbles and small groups of bubbles (bubble swarms) are considered. This is a continuation of our previous studies on the two-bubble coalescence and vortex shedding [32]. The proposed numerical method allows us to simulate a wide range of flow regimes, accurately capturing the shape of the deforming interface of the bubble and the surface tension effect, while maintaining the mass conservation. The computed time-evolution of bubble's position and rise velocity shows a good agreement with the available experimental data. At the same time, the results on the dynamics of bubble interface area, which are, up to our knowledge, presented for the first time, show how much the overall mass transfer would be affected by the interface deformation in the case of the bubble dissolution. Another set of experiments that are of interest for chemical engineers modelling bubbly flows concerns the bubble swarms and their behavior in different bubble-shape regimes. The ellipsoidal and spherical shape regimes are considered to represent, respectively, the coalescing and non-coalescing bubble swarms. The average rise velocities of the bubble swarms are computed and analysed for both regimes.

Keywords: two-phase flow, bubble dynamics, free moving boundary, rise velocity, bubble swarm

1 Introduction

Bubbly flows are central to many industrial and natural processes, and an inter-bubble interaction plays a fundamental role in such flows. Coalescence and breakup can control the interfacial area and mass transfer rate in bubble columns and gas-sparged chemical and biological reactors. However, the actual mechanisms of bubble interactions are not well understood; to find the main factors affecting these mechanisms in bubbly flows, one has to analyze the flow patterns around single rising bubbles and small groups of bubbles. This paper presents the results of a computational study that provides new insights into the phenomena. We compare experimental observations with the simulation results and study, to what extent the physical mechanisms may be explained by the model and numerical methods employed.

*Institute of Mathematics, Zurich University, Winterthurerstrasse 190, CH-8057 Zurich, Switzerland; *E-mail:* antsmol@amath.unizh.ch

†Laboratory of Applied Mathematics, Lappeenranta University of Technology, P. Box 20, 53851 Lappeenranta, Finland; *E-mail:* heikki.haario@lut.fi

‡Laboratory of Applied Mathematics, Lappeenranta University of Technology, P. Box 20, 53851 Lappeenranta, Finland; *E-mail:* pasi.luukka@lut.fi

The rise of a gas bubble in a viscous liquid is usually accompanied by a significant deformation of the bubble, indicating a complex interplay between fluid convection, viscosity and surface tension. The diverse shapes of the bubble resulting from this deformation cause a large variety of flow patterns around the bubble, and vice versa. A number of experimental studies have addressed this problem. Early studies include the rise of a bubble in an inviscid and a viscous liquid, see [13], [41] [42], [44] and [2]. Approximate theoretical solutions have been obtained for either low [38] or high [22] Reynolds numbers under the assumption that the bubble remains nearly spherical.

Experimental investigations of homogeneous bubbly flows can be found, for example, in [16] and [21], who also examined the turbulence generation in such flows. Earlier experimental work is discussed in both papers. Experiments using a homogeneous "quasi two-dimensional" fluidized bed are described in [29]. In computational studies, a number of investigators (see, e.g., [34], [43], [5], [39]) used point particles to simulate dilute multiphase flows without resolving the detailed flow field around each particle. In some cases the influence of the particles on the flow was neglected, in other cases the force exerted on the fluid by the particles was added to the right-hand side of the Navier-Stokes equations. The force on each point particle was specified by analytical models for very low and very high Reynolds numbers and by empirical correlations for finite values of the Reynolds number. Recent computational studies have produced correlations for the forces on spherical bubbles, see [20] and [18]. [23] and [19] have presented simulations where the particle size and its wake are accounted for by distributing the effect of the particle over a few grid cells.

When the flow at moderate and high Reynolds numbers is considered, one has to solve the full Navier-Stokes equations for the unsteady flow around each moving particle, resolving the details of boundary layers and wakes. One of the first attempts to compute a detailed flow pattern around a single bubble was the work of [25],[26],[27] who computed the steady-state shapes of axisymmetric bubbles. Later, many researchers conducted two- and three-dimensional simulations of the unsteady motion of deformable bubbles (see, e.g., [36], [28], [40] and the references therein).

For the detailed dynamics of groups of bubbles or particles, the literature is rather limited. The motion of a couple of hundreds of two-dimensional rigid particles was computed in [14]. [9], [10] examined the settling of circular and elliptic particles in a vertical channel, showing both steady-state settling at low Reynolds numbers as well as the "drafting-kissing-tumbling" behavior identified earlier by [11] at higher Reynolds numbers. The same behavior during the settling of hundreds of three-dimensional solid particles has been revealed in the simulations of [12]. Three-dimensional simulations of up to a hundred solid spheres have been also presented by [15]. As to groups of bubbles, [40] and [7], [8] examined the dynamics of two- and three-dimensional bubble arrays at low and moderate Reynolds numbers; earlier, [6] studied the energy transfer in a two-dimensional system of a few hundred bubbles.

In this paper we employ the numerical approach presented in [32] to study in detail the dynamics of a single rising bubble and bubble swarms in various flow regimes. The paper is organized as follows. Section 2 contains the physical setting of the problem and very briefly addresses the numerical algorithm. In section 3 we present the results on typical characteristics of single rising bubbles in order to show the performance of the method. To this end, diverse bubble shapes, terminal velocities and interfacial area evolution are discussed. In section 4, the behavior of bubble swarms in different shape regimes is addressed as well as the corresponding swarms' average rise-velocities. Some concluding remarks can be found in section 5.

2 Physical setting and numerical algorithm

We consider an unsteady laminar flow of two immiscible fluids (this covers the flows of both gas bubbles and liquid drops in another liquid). Both fluids are assumed to be viscous and Newtonian. Moreover, we suppose that the flow is isothermal, thus neglecting the viscosity and density variations due to changes of a temperature field. We also assume that the fluids are incompressible. This view on the modelling of a gas inside of a bubble is standard in the bubble dynamics, since the Mach number of the bubbly flows is always sufficiently small to neglect the gas compressibility (see [1, §3.6] for a thorough discussion on the incompressibility assumption). Presuming, in addition, the fluids to be homogeneous, we may infer that the densities and viscosities are constant within each fluid. We utilize the sharp-interface (zero interfacial thickness) approach; the density and viscosity have, therefore, a jump discontinuity at the interface (see, e.g., [1]). We assume that the interface has a surface tension. We also suppose that there is no mass transfer through the interface (i.e. the interface is impermeable), and there are no surfactants present in the fluids (hence, there is no species transport along the interface). The surface tension coefficient is, thus, assumed constant.

As a simulation tool we employ a general computational strategy proposed in [30] (see also [31]), that is capable of modelling diverse types of two-fluid interfacial flows. The dynamics of a gas bubble in a liquid can, thus, be considered as a particular application of this computational approach.

We refer to [31] for the mathematical setting of the problem and the details of the numerical algorithm; we notice only that we solve the incompressible Navier-Stokes equations by the fractional-step method using finite element discretization in space and move the bubble interface with the help of the finite element level-set approach.

3 Bubble rise velocity, position and interface area for different shape regimes

In this section, we are concerned with the dynamics of a single rising bubble. We start with the simulation of different bubble-shapes, depending on the values of the physical parameters, to illustrate the performance of our numerical approach and to highlight the main shape-regimes used to classify the bubble behavior. Next, the quantitative comparison of the bubble position and rise velocity as the functions of time with the available experimental data is shown to confirm the ability of the algorithm to deliver the correct information on the typical global characteristics of single rising bubbles. Finally, we analyze the dynamics of the bubble interface area during the bubble rise; this information can be very important for the evaluation of the mass transfer through the bubble surface in the problem of bubble dissolution.

3.1 Bubbles in different shape regimes

The problem of a gas bubble rising due to the buoyancy force in an infinite liquid medium may be characterized by the following eight independent dimensional quantities: the densities ρ_1 and ρ_2, the viscosities μ_1 and μ_2, the gravitational acceleration g, the coefficient of surface tension σ, and the space and time variables. Here the index "1" corresponds to the fluid surrounding the bubble, index "2" to the fluid inside of the bubble. According to the Π-theorem of dimensional analysis, five independent non-dimensional parameters can be formed to completely describe the problem. Those are, usually, the density ρ_1/ρ_2 and

viscosity μ_1/μ_2 ratios, the non-dimensional time $T = t\mu_1/\rho_1 {d_e}^2$, and two of the following three quantities:

$$M = \frac{g\mu_1^4}{\rho_1\sigma^3}, \quad Eo = \frac{gd_e^2\rho_1}{\sigma}, \quad Re = \frac{\rho_1 d_e U}{\mu_1}, \tag{1}$$

which represent the Morton, the Eötvös and the Reynolds numbers, respectively. Here the characteristic length $d_e = \sqrt[3]{\frac{6V}{\pi}}$ is the volume-equivalent diameter of a bubble of volume V, and U denotes the characteristic rise velocity of the bubble. Another dimensionless parameter, the Weber number $We = \frac{\rho_1 U^2 d_e}{\sigma}$, is often used instead of the Eötvös number. It is obvious that Eo and M are the parameters known a priori, while Re and We require a definition of U. If we set $U = \sqrt{gd_e}$, which is a common choice in the literature, we immediately find the explicit relation $M = Eo^3/Re^4$ showing the dependence of the Morton number on the Eötvös and Reynolds numbers.

Although the motion of a buoyant bubble through a viscous liquid always presents an unsteady process, there is a possibility to divide all possible flow patterns into several different groups, called "shape regimes", characterized by the assumption that within each regime the bubble retains nearly the same shape. A particular "representative" shape of the bubble can be realized only some time after the initially spherical bubble starts its evolution; on the other hand, at later stages of the motion, the bubble shape may change so significantly that we may probably speak of a transition from one shape regime to another. So, the notion of the shape regimes is somewhat rough, though it has been proved extremely useful for classification of different types of bubble behavior. In light of the above, the non-dimensional time T indicating an explicit temporal dependence can be neglected for a time being; then, the whole problem remains governed by four non-dimensional parameters, which we take, following [4], to be the density ratio, the viscosity ratio, the Eötvös number and either the Morton or the Reynolds number.

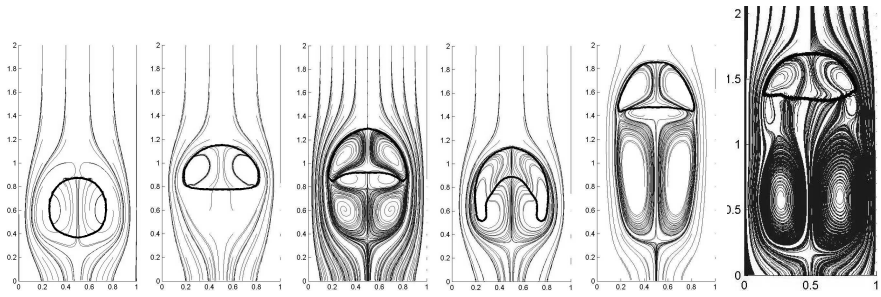

(a) (b) (c) (d) (e) (f)

Figure 1: Different computed shapes of bubbles: (a) spherical: Re=1, Eo=0.6, (b) ellipsoidal: Re=20, Eo=1.2, (c) dimpled ellipsoidal cap: Re=35, Eo=125, (d) skirted: Re=55, Eo=875, (e) spherical cap: Re=94, Eo=115, (f) wobbling: Re=1100, Eo=3.0; $\rho_1/\rho_2 = 10^3$; $\mu_1/\mu_2 = 10^2$.

The typical bubble shapes and velocity streamlines in the frame of reference of the bubble are shown in Figure 1. These numerical bubble shapes are in a good agreement with the experimental predictions of [2] and [4]. It is worth noting that all basic shapes are successfully recovered with the physical parameter values lying exactly within the limits given in [4].

3.2 Terminal velocity of the bubble

The notion of the terminal velocity of a rising bubble is, to some extent, vague. In reality, the Archimedian force, the drag, the lift and the virtual mass forces exerted on the bubble never balance each other, and, thus, the bubble motion always remains unsteady. However, if the bubble motion is considered in an infinite fluid-medium, after some period of time we may speak of a certain average "rise velocity", whose change in time can be neglected. The averaging is meant here over a time interval much shorter than the period of time passed since the beginning of the bubble motion. Therefore, under the terminal velocity we understand such a time-averaged ("smoothed") rise velocity of the bubble.

The terminal velocity of a rising bubble has been experimentally measured by many investigators. The measured terminal velocities differ widely, mainly due to the differences in system's purity. For instance, some researchers have noticed a strong influence of system's purity on the drag or terminal velocity, while the viscosity of internal fluid may be of secondary importance in the presence of uncontrolled surfactant effects. For practical predictions, it is useful to have the terminal velocity correlated explicitly in terms of system variables. Clift et al. ([4]) determined the terminal velocity for a rising bubble as $U_T = \frac{\mu}{\rho d_e} M^{-0.149}(J - 0.857)$, where $J = 0.94H^{0.757}$ for $2 < H \leq 59.4$ and $J = 3.42H^{0.441}$ for $H > 59.4$. Here $H = \frac{4}{3} Eo\, M^{-0.149}(\frac{\mu}{\mu_w})^{-0.14}$ and μ_w is the viscosity of water, which may be taken as 0.09 $kg/m \cdot s$. It is important to note that the density and viscosity of the fluid inside of the bubble are not included in the correlation; ρ and μ denote here the parameters of the surrounding fluid.

A more recent equation for the terminal velocity has been reported by Rodrigue ([24]) as $U_T = V/(\frac{d_e \rho^2}{\sigma \mu})^{1/3}$, where $V = \frac{aF^b}{1+cF^d}$ and $F = g(\frac{d_e^8 \rho^5}{\sigma \mu^4})^{1/3}$ with fitted parameter values $a = 1/12$, $b = 1$, $c = 0.049$, $d = 3/4$.

In Table 1 we have compared the results computed by the above mentioned formulae of Clift et al. and of Rodrigue with the results of our calculations. We computed the bubble rise velocity as the velocity of the top of the bubble.

Bubble shape	Clift et al.	Rodrigue	our results
Spherical cap	0.3717	0.5349	0.58
Dimpled ellipsoidal	0.8271	0.9581	0.62
Skirted	0.5996	0.7957	0.71
Spherical	0.3253	0.0806	0.04
Ellipsoidal	0.6064	1.5011	0.42

Table 1: Terminal velocity for different shape regimes. The comparison with the formulae of Clift et al. ([4]) and Rodrigue ([24]).

If compared to Rodrigue's results, our terminal velocities differ most in ellipsoidal and dimpled ellipsoidal shape regimes, where it is experimentally difficult to find accurate predictions. Otherwise, the results seem to agree reasonably well. In all but one (spherical) case the values of Clift et al. are also rather close to ours. It is worth noticing again that in the formulae of Clift et al. and of Rodrigue the dependence of the terminal velocity on the viscosity/density of the internal fluid is neglected; this is not the case in our simulations.

The smoothed rise velocities for different shape regimes are shown in Figure 2, indicating that the smallest terminal velocity is exhibited by the spherical bubble, while the greatest is demonstrated by the dimpled ellipsoidal-cap and by the skirted bubbles. Figure 3 illustrates the oscillating character of the rise velocity. The oscillations reflect the complex interplay of diverse forces influencing the bubble motion; the magnitude of the

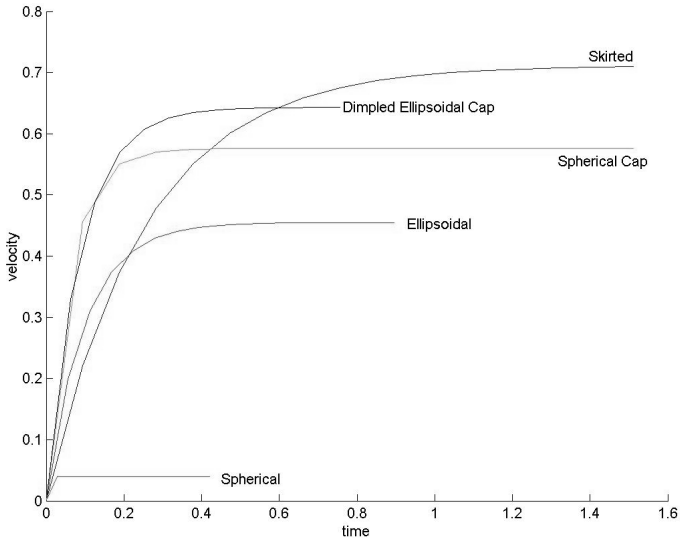

Figure 2: Smoothed rise velocities vs. time for different shape regimes.

oscillations is larger for more "stiff" bubbles, i.e. for the bubbles which are more resistant to the deformations.

3.3 The bubble position versus time

Figure 4 shows the height of the bubble top as a function of time. The considered shape regimes are skirted, spherical-cap, dimpled ellipsoidal-cap and ellipsoidal. It is clearly seen that in the case of higher Reynolds numbers (spherical-cap, skirted) the bubble rises faster than in the regimes with lower Reynolds numbers (ellipsoidal-type shapes). We see that, at the starting moment, the bubble position changes slowly, but, later, the height of the bubble top grows almost linearly with time. Qualitatively, our results compare well with the results of [37] (see Figure 11 in [37], where the same temporal dependence is observed). [3] have also reported analogous numerical results (see Figures 5, 12, 16, 18 in [3]), demonstrating the same linear dependence of the bubble position on time. Both [37] and [3] found that their results agree with the available experimental data.

3.4 Interface area of a bubble

To our knowledge, there have been no investigations on the evolution of the bubble surface area, although such results can be of primary importance, for example, in estimating the total mass transfer across the surface of a dissolving gas bubble. While the bubble volume is conserved in our model owing to the incompressibility assumption, the area (the length in 2D) of the bubble interface may undergo rather dramatic changes during the bubble motion.

In this section we study the behavior of the relative interfacial length as a function of time. Under the relative length of the bubble interface we understand the length of the interface at each time moment divided by the length of the initial, circular interface. As it is seen in Figure 5, the relative interfacial length of the bubble remains close to 1 when a spherical bubble is concerned. An ellipsoidal bubble has a very small increase in the relative length. A dimpled ellipsoidal-cap bubble, first, has a bigger change in the relative

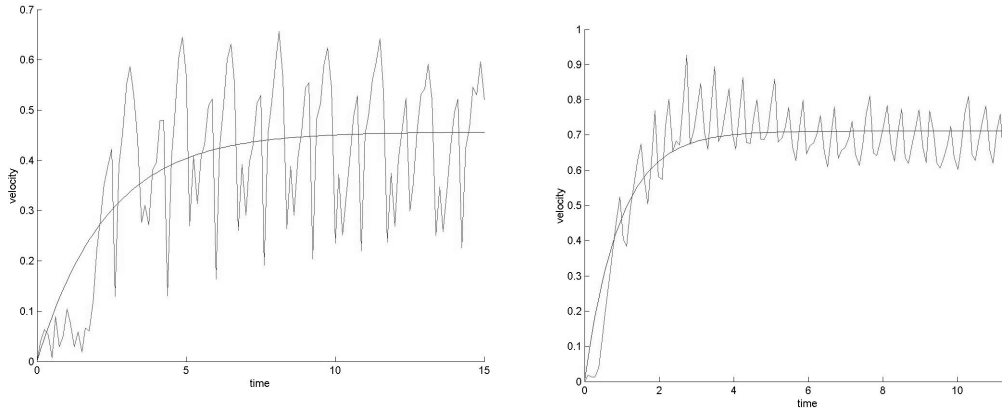

(a) (b)

Figure 3: Rise velocity vs. time for (a) ellipsoidal and (b) skirted bubble: original and smoothed.

interfacial length, then the surface length gets smaller and, finally, tends to a certain limit value. This kind of oscillation occurs due to the fact that the bubble first tries to achieve a skirted shape but, at later times, eventually reaches a dimpled ellipsoidal shape, where it remains. In the skirted case, the breakup of the bubble is clearly observed on the graph of the relative interfacial length. Right before the moment of the breakup the relative length is almost 2, which means that the interface length is twice its initial value. After the bubble breaks, the relative length goes closer to 1, then the bubble starts to regain the skirted shape and the interfacial length increases again. With a spherical-cap bubble the relative length first almost reaches the value 2 (at this point the bubble is skirted and about to break) and then, after the breakage, the relative length goes back to about 1.4, and the bubble recovers the spherical-cap shape. It is important to note that, after each breakup, we obtain several "child" bubbles, and each of them has a volume smaller than the volume of the "parent" bubble. This means that each "child" bubble has a correspondingly smaller Eötvös number, i.e. its interface is more resistant to possible deformation and stretching. Thus, the total interfacial length should always tend to some limit value, as in the case of a nearly ellipsoidal bubble shape.

4 Bubble swarms

While the dynamics of a single bubble is important for understanding the processes in bubbly flows, yet more useful information can be extracted from the analysis of the rise of small groups of bubbles. Although the groups of approximately 10 bubbles are not, of course, representative enough to model a bubbly flow, they can be used to evaluate (at least, qualitatively) some macroscopic characteristics of the multiphase flow, like, e.g., the so-called "gas-slip velocity" (see [17], [33]). This velocity is used in the macroscopic models for the multiphase flows, and some empirical correlations are usually invoked for its estimation. In this section we try to make the first steps toward establishing the laws governing the dynamics of the gas-slip velocity by analyzing the average rise velocity of bubble swarms in two different shape regimes. We also thoroughly consider the behaviour of individual bubbles in a swarm and of a bubble swarm as a whole, having in mind the

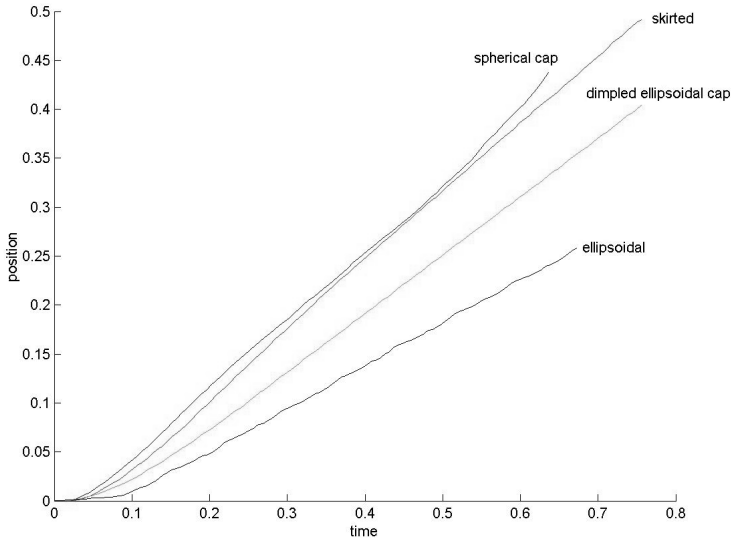

Figure 4: Bubble position vs. time for ellipsoidal, dimpled ellipsoidal-cap, spherical-cap and skirted shape regimes.

importance of the dynamics of this intermediate, bubble-swarm scale for understanding the bubbly flows at the macro-level.

In the numerical experiments, we consider nine bubbles arranged in a sort of "array": the lower and the middle "rows" consist of three bubbles side by side, in the upper "row" the central bubble is placed slightly above others to break the symmetry. All bubbles are initially spherical and of equal size.

It is known (see, e.g., [35]) that the behavior of a bubble swarm essentially depends on the Morton number (M) of the liquid: in "low-M" liquids the bubbles tend to coalesce within a swarm, while in "high-M" liquids the bubbles form clusters but do not merge. The transition between "coalescing" and "non-coalescing" regimes is not sharp and hard to capture experimentally; in [35], the threshold $M \approx 4 \cdot 10^{-4}$ was proposed. Below we consider the ellipsoidal and spherical shape regimes corresponding to relatively small and large Morton numbers, respectively. It is worth noting that, in the numerical simulations, the effect of bubble coalescence strongly depends on the grid resolution. That is why in both cases we compute on the grids with the same width $h = 1/80$.

4.1 Bubble swarms in ellipsoidal shape regime

Bubble swarm rising in ellipsoidal shape regime can be seen in Figures 6 – 8. Here, the Reynolds and Eötvös numbers are 20 and 1.2, correspondingly, which yields the Morton number $M = 1.1 \cdot 10^{-5}$. For such a small M one can expect multiple coalescences and mergers of the bubbles in a swarm, and this is exactly what we are about to see.

First, the top bubble starts to rise fast and two other bubbles in the top row start approaching each other. At the same time, the near-wall bubbles in the middle row begin to rise faster, while the center bubble rises slower (Figure 6(c)); this effect is caused by the wake of the top-row bubbles. In the lowest row an opposite phenomenon is observed: the center bubble rises faster than the two other. After a short time, the center bubble in the middle row becomes strongly influenced by its 'neighbors' which have risen above it and the lowest center bubble reaches its wake (see Figure 6(d)). In the next moment,

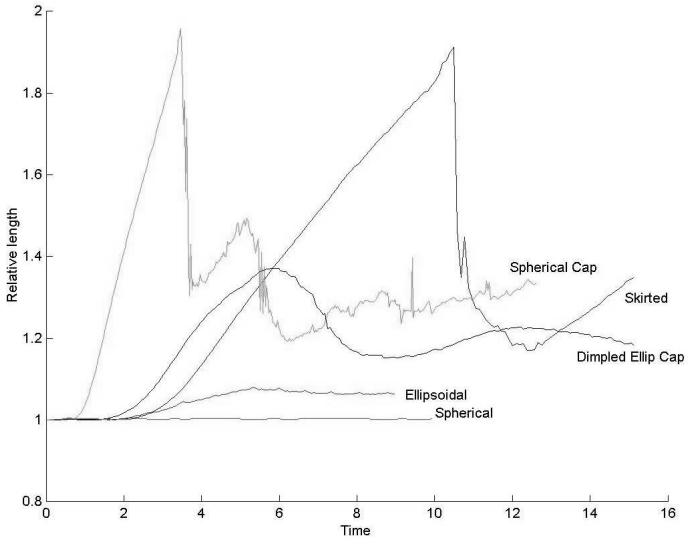

Figure 5: Relative interfacial lengths for different shape regimes. The bubble evolves from the spherical to its final rising shape.

the center bubble in the middle row stretches in the horizontal direction and merges with the lowest center bubble. After the merging, the bubble still continues getting wider and upper bubbles' wakes cause it to form a neck-like shape and, finally, to break in the middle. At this time-point, both upper and lower bubbles have come very close to each other, but a merger does not occur when the bubbles are side by side: the bubbles rise steadily in groups of two (except the most upper bubble that rises alone). In [35], it is reported that "... when several bubbles were captured in the wake of another simultaneously or in a rapid sequence, they formed a cluster". At this point of our simulation we can clearly see this effect (see Figures 6(i), 7(a),(b)). Such a type of cluster forming is also known to be the basic foundation for the transition from bubbly to slug flow.

It is also noticed in [35] that "... if large number of bubbles (say $5 - -10$) were involved, they formed a 'chimney' in which a cluster's wake was strong enough to sustain itself by continually gathering in new bubbles to replace possibly dispersed ones". In our simulations, the cluster of bubbles forming a "chimney" can be clearly seen (see Figure 7(c)). Now, the bubble groups form a pronounced wake behind them. A wake was not observed in this regime when the rise of a single bubble was studied. When the lower bubbles get closer to the upper ones, a bubble coalescence begins. First, the upper group of two bubbles merges with the leading bubble and, at the same time, the group of six evolves into a group of five, when two upper bubbles on the left-hand side merge together. Next, a coalescence occurs on the right-hand side of this group of five when the two lowest bubbles merge (see Figure 7(g) and note the non-symmetric character of the merger process). At this moment, the leading bubble is reached by others; the coalescence with the "leader" starts on the right-hand side of the bubble group (see Figures 7(h),(i) and 8(a)-(c)). This unsymmetric coalescence process makes the final big bubble wobble from side to side, which, in its turn, results in an unsymmetric wake behind the bubble (and vice versa, the asymmetry of the wake causes the wobbling-type motion of the bubble, see Figures 8(d)-(h)). This kind of the bubble behavior agrees well with the experimental studies of [35] where it is reported that "... as chimney grew, stronger coalescences encouraged by

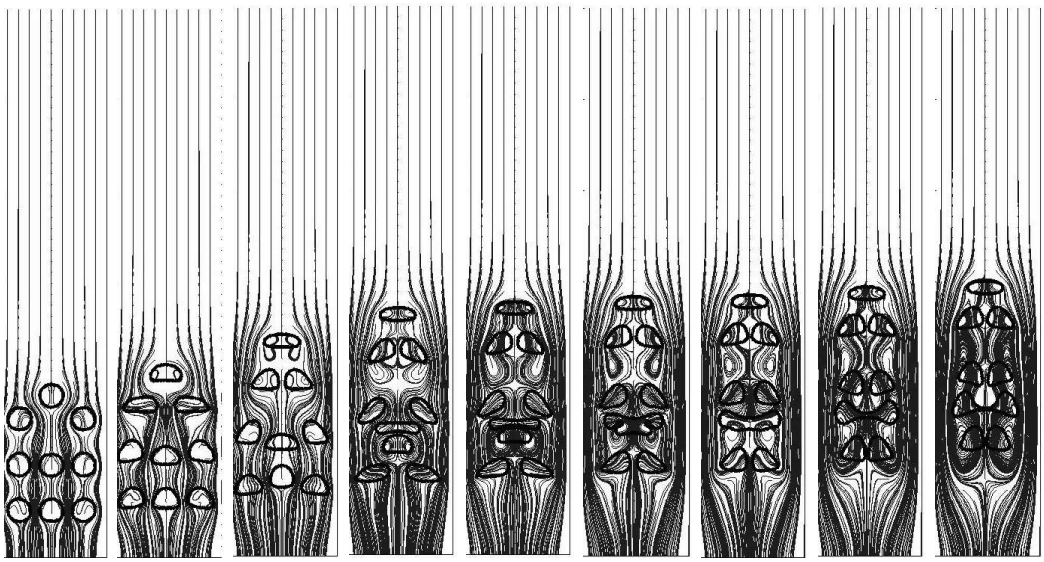

(a) (b) (c) (d) (e) (f) (g) (h) (i)

Figure 6: Bubble swarm in ellipsoidal shape regime; $Re = 20$, $Eo = 1.2$, $M = 1.1 \cdot 10^{-5}$, $\rho_1/\rho_2 = 10^3$, $\mu_1/\mu_2 = 10^2$.

the close proximity of bubbles in the cluster created large caps".

Our results also compare well with the results of [40] at the point that, in some cases, the nearly uniform bubble distribution undergoes a transition to a completely different state where the bubbles accumulate in vertical streams, rising much faster than when they are uniformly distributed.

In Figure 9 one can see average rise velocities of bubble swarms with four different density ratios. Average velocities here are simply the arithmetic means of individual bubble velocities in a swarm. Figures 6 – 8 represent the simulation with the density ratio equal to 1000 that can be viewed as the case of the fastest rising bubble swarm. An increase of the gas density (i.e. a decrease of the density ratio) lowers the bubble buoyancy, which ultimately implies smaller rise velocities of bubble swarms. The velocity profiles in Figure 9 differ from those of single rising bubbles (see Figure 2); one can also notice that the average rise velocity of a swarm of ellipsoidal bubbles is clearly greater than the rise velocity of any bubble from the swarm, if this bubble would rise alone (see Table 1). This confirms the statement that the bubbles rise faster in a cluster. This effect can also be seen in Figure 9 for density ratios equal to 20 and 100: the swarm rise velocity grows up till the moment when the bubble mergers result in a creation of a large leading bubble; at this moment, the rise velocity starts to fall down to the level of the terminal velocity of the correspondingly large, single ellipsoidal bubble.

4.2 Bubble swarms in spherical shape regime

In this set of numerical experiments, we used the values of the Reynolds and Eötvös numbers $Re = 1$ and $Eo = 0.63$, which results in the Morton number $M = 0.25$ that is greater than the threshold value and, thus, must imply the "non-coalescing" rise of the bubble swarm. The density ratio of liquid and gas was $\rho_1/\rho_2 = 1000$, the viscosity ratio $\mu_1/\mu_2 = 20$.

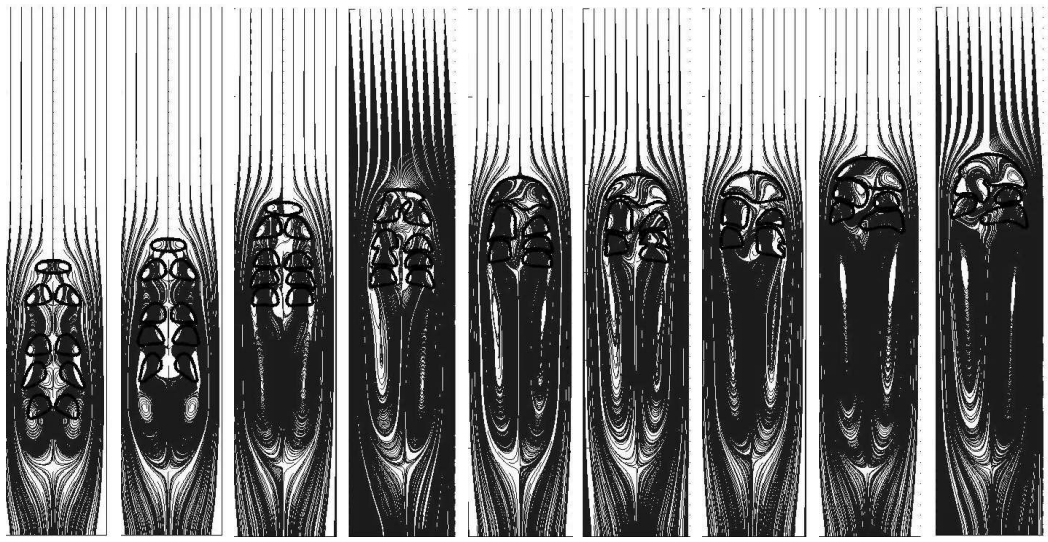

(a) (b) (c) (d) (e) (f) (g) (h) (i)

Figure 7: Bubble swarm in ellipsoidal shape regime (contin.); $Re = 20$, $Eo = 1.2$, $M = 1.1 \cdot 10^{-5}$, $\rho_1/\rho_2 = 10^3$, $\mu_1/\mu_2 = 10^2$.

As seen in Figure 10, the bubbles tend to form clusters but do not merge. The bubbles at the center of the computational domain start rising much faster than the bubbles near the boundaries (see Figure 10(b)). This is in contrast to the ellipsoidal shape regime where the wake of the upper bubbles slowed down the initial acceleration of the bubbles in the center. The uppermost bubble at the center rises faster than others, leaving them behind. Also, other two center bubbles form a cluster and reach the upper bubbles near the boundaries rather fast. Bubbles in clusters of two seem first to get closer, then again take distance from each other. This kind of back and forth motion was observed with several two-bubble clusters. When a two-bubble cluster reaches another one, they form together a four-bubble cluster and start to rise as a whole (Figures 10(g),(h)). It is worth noticing that, exactly as in the case of a single spherical bubble, no significant wake can be observed behind the bubbles.

The individual bubble rise velocities are shown in Figure 11(a). The average rise velocity of the swarm is indicated by a thick line. In Figure 11(b) we have fitted the average swarm velocity to an exponential type curve to see the similarity of the velocity behavior with that of a single spherical bubble. However, the terminal swarm velocity (here, approximately, 0.44) is definitely greater than the terminal velocity of a single spherical bubble having the same size as the bubbles in the swarm (see Table 1).

5 Concluding remarks

In this paper, we have continued our previous research on numerical modelling of bubble dynamics. The work has been focused on the computation of typical global characteristics of single rising bubbles (such as the time-evolution of the bubble interface area, bubble's position and rise velocity) as well as on the simulation of bubble groups in different shape regimes. A good qualitative agreement with the experimental data has been always observed, and the numerical results for the terminal velocities seem to be reasonably close to

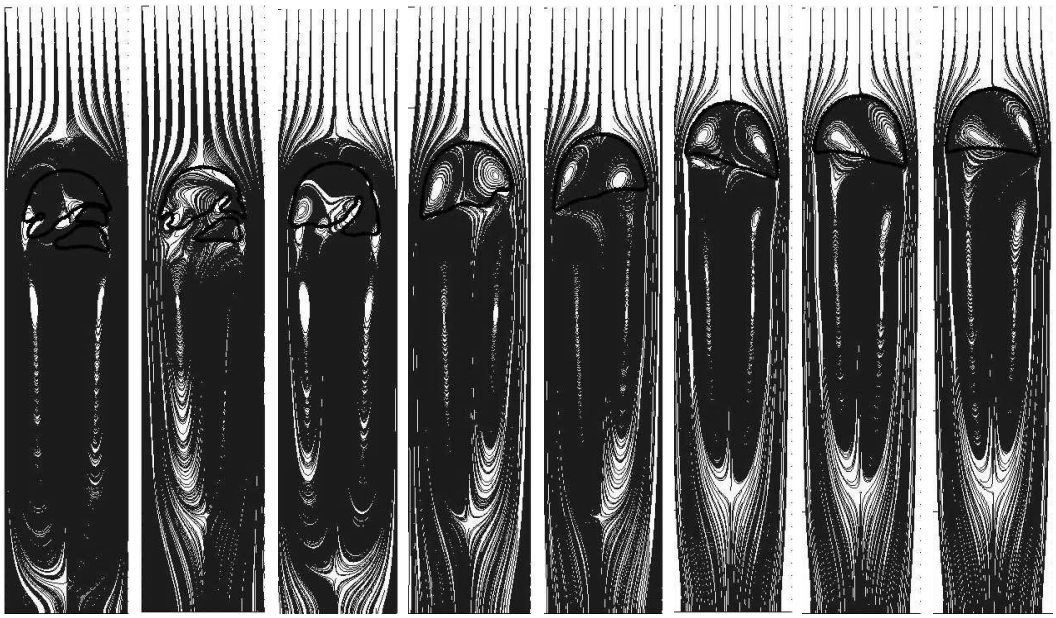

(a) (b) (c) (d) (e) (f) (g) (h)

Figure 8: Bubble swarm in ellipsoidal shape regime (contin.); $Re = 20$, $Eo = 1.2$, $M = 1.1 \cdot 10^{-5}$, $\rho_1/\rho_2 = 10^3$, $\mu_1/\mu_2 = 10^2$.

the available empirical correlations derived from the experimental values. Unfortunately, we are unaware of any results on the dynamics of the bubble interface area, although these results are important for the evaluation of total mass transfer through the surface of a dissolving bubble. Our numerical predictions indicate that at moderate and high Reynolds numbers (skirted and spherical-cap shape regimes) the total interface area exhibits large-amplitude oscillations and may increase as much as in 2 times at some time moments. The simulations of bubble swarms in ellipsoidal and spherical shape regimes confirm the dependence of the swarm dynamics on the Morton number of the liquid: at low Morton numbers the bubbles intensively coalesce in a swarm, tending to create a single large bubble, while at high Morton numbers no mergers have been observed. This suggests that the high Morton number regimes lead to a greater total interface area (i.e. the sum of interface areas of all bubbles in the swarm) and, hence, might be more advantageous from the viewpoint of mass transfer. Since the Morton number is inversely proportional to the 4th power of the Reynolds number, there is some trade-off here with our predictions of a bigger interface area at high Reynolds numbers for individual bubbles. The quantitative assessment of the average rise velocities of the swarms shows that these velocities are always greater than the terminal velocities of single bubbles, thus, confirming that the bubbles rise faster in clusters.

The presented computational studies demonstrate the abilities of numerical simulations to deliver useful information on the dynamics of bubble swarms. However, further work is needed to systematically study the swarms in all shape regimes and to derive the corresponding correlation for the swarm average velocity.

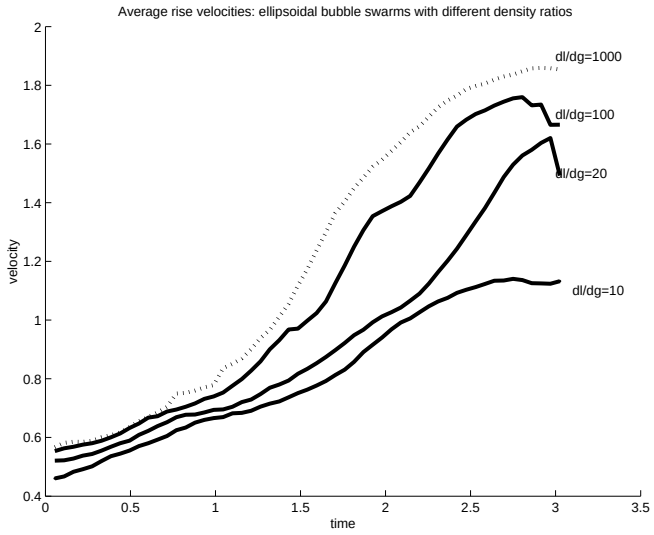

Figure 9: Average rise velocities of bubble swarms in ellipsoidal shape regime; $Re = 20$, $Eo = 1.2$, $\rho_1/\rho_2 = 10,\ 20,\ 100,\ 1000,\ \mu_1/\mu_2 = 10^2$.

References

[1] G.K. Batchelor, An Introduction to Fluid Dynamics. Cambridge University Press, 1967.

[2] D. Bhaga, M. E. Weber. Bubbles in viscous liquids: shapes, wakes and velocities. J. Fluid Mech. 105 (1981), 61–85.

[3] L. Chen, S.V. Garimella, J.A.Reizes, E. Leonardi. The development of a bubble rising in a viscous liquid. J. Fluid Mech. 387 (1999), 61–96.

[4] R.C. Clift, J.R. Grace, M.E. Weber. Bubbles, Drops and Particles. Academic Press, 1978.

[5] S. Elghobashi, G. C. Truesdell. On the two-way interaction between homogeneous turbulence and dispersed solid particles. I: Turbulence modification. Phys. Fluids A, 15 (1993), 1790–1801.

[6] A. Esmaeeli, G. Tryggvason. An inverse energy cascade in two-dimensional, low Reynolds number bubbly flows. J. Fluid Mech. 314 (1996), 315–330.

[7] A. Esmaeeli, G. Tryggvason. Direct numerical simulations of bubbly flows. Part 1. Low Reynolds number arrays. J. Fluid Mech. 377 (1998), 313–345.

[8] A. Esmaeeli, G. Tryggvason. Direct numerical simulations of bubbly flows Part 2. Moderate Reynolds number arrays. J. Fluid Mech. 385 (1999), 325–358.

[9] J. Feng, H. H. Hu, D. D. Joseph. Direct simulation of initial value problems for the motion of solid bodies in a Newtonian fluid. Part 1. Sedimentation. J. Fluid Mech. 261 (1994), 95–134.

[10] J. Feng, H. H. Hu, D. D. Joseph. Direct simulation of initial value problems for the motion of solid bodies in a Newtonian fluid. Part 2. Couette and Poiseuille flows. J. Fluid Mech. 277 (1995), 271–301.

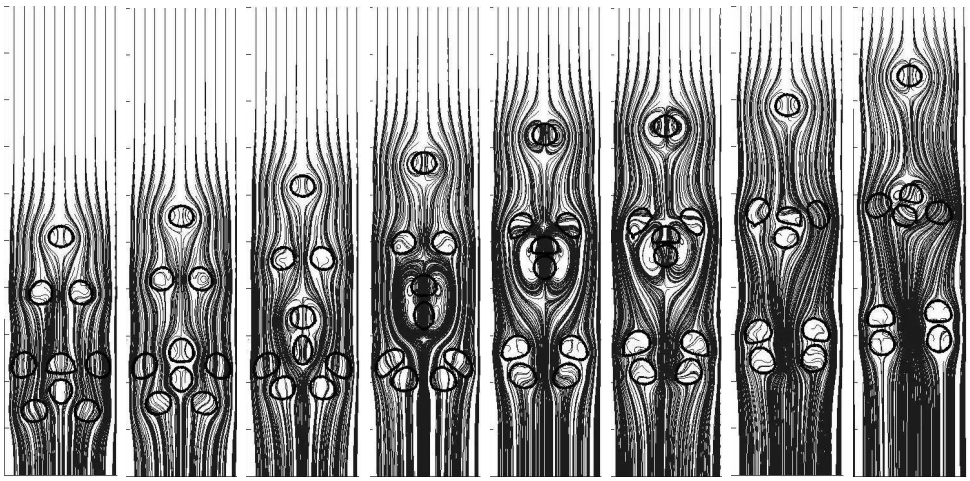

(a) (b) (c) (d) (e) (f) (g) (h)

Figure 10: Bubble swarm in spherical shape regime; $Re = 1$, $Eo = 0.63$, $M = 0.25$, $\rho_1/\rho_2 = 10^3$, $\mu_1/\mu_2 = 20$.

[11] A. Fortes, D. D. Joseph, T. Lundgren. Nonlinear mechanics of fluidization of beds of spherical particles. J. Fluid Mech. 177 (1987), 467–483.

[12] R. Glowinski, T.-W. Pan, T. I. Hesla, D.D. Joseph. A distributed Lagrange multiplier/fictitious domain method for particulate flows, Int. J. Multiphase Flow 25 (1999), 755–794.

[13] R. A. Hartunian, W. R. Sears. On the instability of small gas bubbles moving uniformly in various liquids. J. Fluid Mech. 3 (1957), 27–47.

[14] H. H. Hu. Direct simulations of flows of solid-liquid mixtures. Int. J. Multiphase Flow 22 (1996), 335–349.

[15] A. A. Johnson, T. E. Tezduyar. 3D simulation of fluid-particle interactions with the number of particles reaching 100. Comput. Meth. Appl. Mech. Engng. 145 (1997), 301–321.

[16] M. Lance, J. Bataille. Turbulence in the liquid phase of a uniform bubbly air-water flow. J. Fluid Mech. 222 (1991), 95–118.

[17] A. Lapin, A. Lübbert. Numerical simulation of the dynamics of two-phase gas-liquid flows in bubble columns. Chem. Eng. Sci. 49, no. 21, (1994), 3661–3674.

[18] J. M. Magnaudet, I. Eames. The motion of high-Reynolds-number bubbles in inhomogeneous flows. Ann. Rev. Fluid Mech. 32 (2000), 659–708.

[19] M. R. Maxey, B. K. Patel. Forced-coupled simulations of particle suspensions at zero and finite Reynolds numbers. J. Fluid Mech. 256 (1997), 647–683.

[20] R. Mei. Velocity fidelity of flow tracer particles. J. Fluid Mech. 22 (1996), 1–13.

[21] M. Mizukami, R. N. Parthasarathy, G. M. Faeth. Particle-generatied turbulence in homogeneous dilute dispersed flows. Int. J. Multiphase Flow 18 (1992), 397–412.

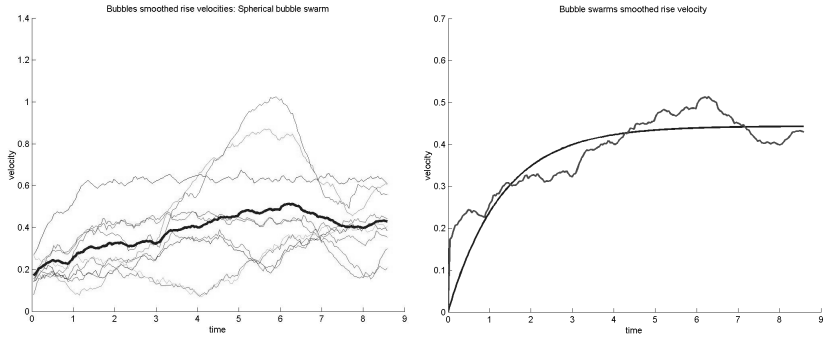

(a) (b)

Figure 11: (a) Rise velocities of individual bubbles (thin lines) and average rise velocity of the swarm (thick line); (b) The smoothed and fitted average rise velocity of the swarm; $Re = 1$, $Eo = 0.63$, $M = 0.25$, $\rho_1/\rho_2 = 10^3$, $\mu_1/\mu_2 = 20$.

[22] D. W. Moore. The rise of a gas bubble in a viscous liquid. J. Fluid Mech. 6 (1959), 113–130.

[23] Y. Pan, S. Banarjee. Numerical investigation of the effect of large particles on wall-turbulence. Phys. Fluids 9 (1997), 3786–3807.

[24] D. Rodrigue. Generalized correlation for bubble motion. AIChE J. 47 (2001), 39–44.

[25] G. Ryskin, L.G. Leal. Numerical solution of free-boundary problems in fluid mechanics. Part 1. The finite-difference technique. J. Fluid Mech. 148 (1984), 1–17.

[26] G. Ryskin, L.G. Leal. Numerical solution of free-boundary problems in fluid mechanics. Part 2. Buoyancy-driven motion of a gas bubble through a quiescent liquid. J. Fluid Mech. 148 (1984), 19–35.

[27] G. Ryskin, L.G. Leal. Numerical solution of free-boundary problems in fluid mechanics. Part 3. Bubble deformation in an axisymmetric straining flow. J. Fluid Mech. 148 (1984), 37–43.

[28] R. Scardovelli, S. Zaleski. Direct numerical simulation of free-surface and interfacial flow. Ann. Rev. Fluid Mech. 31 (1999), 567–603.

[29] P. Singh, D. D. Joseph. Dynamics of fluidized suspension of spheres of finite size. Int. J. Multiphase Flow 21 (1995), 1–26.

[30] A. Smolianski. Numerical Modeling of Two-Fluid Interfacial Flows. PhD thesis, University of Jyväskylä, ISBN 951-39-0929-8, 2001.

[31] A. Smolianski. Finite-element/level-set/operator-splitting (FELSOS) approach for computing two-fluid unsteady flows with free moving interfaces. Int. J. Num. Meth. Fluids 48, no. 3, (2005), 231–269.

[32] A. Smolianski, H. Haario, P. Luukka. Vortex shedding behind a rising bubble and two-bubble coalescence: a numerical approach. Appl. Math. Modelling, in press.

[33] A. Sokolichin, G. Eigenberger. Gas-liquid flow in bubble columns and loop reactors: Part I. Detailed modelling and numerical simulation. Chem Eng. Sci. 49, no. 24B, (1994), 5735–5746.

[34] K. D. Squires, J. K. Eaton. Particle response and turbulence modification in isotropic turbulence. Phys. Fluids A 2 (1990), 191–203.

[35] C.W. Stewart. Bubble interaction in low-viscosity liquids. Int. J. Multiphase Flow 21 (1995), 121–132.

[36] M. Sussman, P. Smereka. Axisymmetric free boundary problems. J. Fluid Mech. 341 (1997), 269–294.

[37] M. Sussman, P. Smereka, S. Osher. A level set approach for computing solutions to incompressible two-phase flow. J. Comput. Phys. 114 (1994), 146–159.

[38] T.D. Taylor, A. Acrivos. On the deformation and drag of a falling viscous drop at low Reynolds number. J. Fluid Mech. 18 (1964), 466–476.

[39] G. C. Truesdell, S. Elghobashi. On the two-way interaction between homogeneous turbulence and dispersed solid particles. II: Particle dispersion. Phys. Fluids A 6 (1994), 1405–1411.

[40] G. Tryggvason, B. Bunner, A. Esmaeeli, D. Juric, N. Al-Rawahi, W. Tauber, J. Han, S. Nas, Y.-J. Jan. A Front Tracking Method for the Computations of Multiphase Flow. J. Comput. Phys. 169 (2001), 708–759.

[41] J.K. Walters, J.F. Davidson. The initial motion of a gas bubble formed in an inviscid liquid. Part 1. The two-dimensional bubble. J. Fluid Mech. 12 (1962), 408–417.

[42] J.K. Walters, J.F. Davidson. The initial motion of a gas bubble formed in an inviscid liquid. Part 2. The three-dimensional bubble and the toroidal bubble. J. Fluid Mech. 17 (1963), 321–336.

[43] L. P. Wang, M. Maxey. Settling velocity and concentration distribution of heavy particles in homogeneous isotropic turbulence. J. Fluid Mech. 256 (1993), 27–68.

[44] P.P. Wegener, J.Y. Parlange. Spherical-cap bubbles. Ann. Rev. Fluid Mech. 5 (1973), 79–100.